Transactions on the Built Environment vol 66, © 2003 WIT Press, www.witpress.com, ISSN 1743-3509

# Testing and modelling of masonry creep and damage in uniaxial compression

J. Pina-Henriques & P. B. Lourenço
*University of Minho, Portugal*

## Abstract

The problems related to the analysis of ancient constructions are gigantic due to the difficulties in characterizing the geometry, the materials, the sequence of construction, the existing damage and the building processes.

A difficult aspect in the repair and strengthening of existing structures is the long term loading of masonry in compression. Safety assessment has been greatly influenced by the collapse of monumental buildings in the last decade, where creep behaviour and creep-fatigue interaction proved to be of relevance for massive masonry walls. Experimental tests on masonry creep have been recently carried out, together with numerical implementations. Both testing and numerical modelling of multi-leaf masonry walls need still more research.

Experimental testing on the creep of regular ancient masonry together with numerical modelling is currently under investigation and is briefly addressed in the paper. In addition, a discussion of the load transfer between masonry components is given. This represents a contribution for understanding creep behaviour and load transfer mechanisms in multi-leaf walls.

## 1 Introduction

Several times during the centuries, and in different sites, the collapse of a tower took place months or even years after a low intensity shake occurred, without apparently provoking immediate damage to the structure. In other cases of collapse, a clear change in the loading conditions did not occur and the existing damage included apparently minor diffused cracks on the walls. Time-dependent collapse must be assumed in order to explain such phenomena.

Masonry creep depends mainly on factors like state of stress, strength of the material and temperature and humidity conditions, e.g. [1]. Fatigue actions, like

wind and temperature variations, can have a synergetic effect increasing material damage [2]. For these reasons high towers and pillars are the constructions where this phenomenon can more severely occur.

Three stages in creep behaviour can be recognised. In the first one, denominated by primary creep, strain occurs at decreasing rate. At some conditions, the primary creep curve approximates a steady rate of strain called secondary creep. In highly stressed specimens secondary creep may turn upward in tertiary creep, which is characterized by increasing strain rate until creep failure suddenly occurs. In the last two stages diffuse and thin vertical cracking initiates, accompanied by dilatancy, and, only near to failure, larger cracks propagate rapidly and lead to sudden collapse. Long-term tests carried out on specimens from the ruins of the collapsed Civic Tower of Pavia revealed secondary creep showing even at 40% of the estimated strength [3].

The purpose of the present research, jointly carried out by University of Minho (UMinho) and Politecnico di Milano (PoliMi), Italy, is to provide recommendations regarding the strengthening and the safety of historical masonry structures under long-term loading. For this purpose a set of experimental tests and of advanced numerical analyses are to be carried out.

## 2 Description of the experimental programme

Creep tests on regular ancient masonry are in course at Uminho. Pseudo-creep tests on rubble ancient masonry and shear tests on multi-leaf walls are in course at PoliMi. Creep and pseudo-creep tests have already been performed at PoliMi.

### 2.1 Description of the full-creep tests

The tests in course are being carried out on four regular masonry prisms from the collapsed Tower of Pavia, Italy, with dimensions of 200×200×300 $mm^3$. Specially designed test set-ups (Figure 1) are being used and successive load steps of 0.35 $N/mm^2$ are being kept constant for three months. Environment conditions are maintained fairly constant during testing.

The objective of these tests is to get data that, firstly, allow quantifying the viscous parameters that rule the long term behaviour of masonry and, secondly, allow the validation of numerical models. Some preliminary results will be presented during the conference. For the already performed tests see [4].

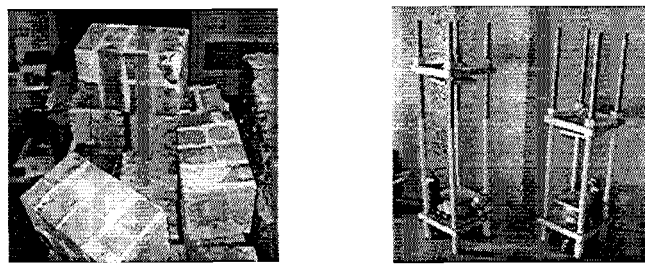

Figure 1: Specimens and set-up for full-creep testing.

### 2.2 Description of pseudo-creep tests

Pseudo-creep tests were carried out recently on six rubble masonry prisms from the Cathedral of Monza, Italy, with dimensions of 200×200×300 mm$^3$. The load was applied in load steps of 0.25 N/mm$^2$, which were kept constant for three hours (Figure 2).

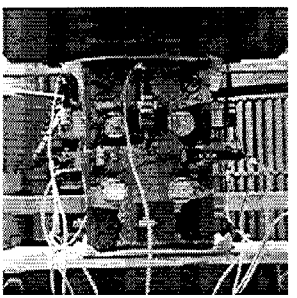

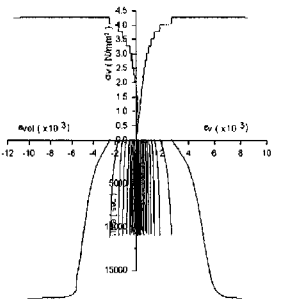

Figure 2: Specimen for pseudo-creep tests and typical obtained data, where the three creep stages can be observed.

### 2.3 Shear tests on multi-leaf wallets

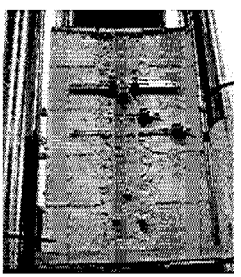

Figure 3: Three-leaf wallet.

Twelve three-leaf wallets (regular-rubble-regular) with dimensions of 300×500×800 mm$^3$ were built (Figure 3). Two types of connection between leaves (with and without indentation) and two types of stone with different mechanical and physical properties have been considered. Monotonic compressive loading will be applied in the inner leaf, being the specimen supported by the external leaves.

The objective of these tests is to evaluate the mechanical behaviour of the connection between leaves and, in this way, estimate the load transference between layers and characterize the stress distribution in the cross section of multi-leaf walls.

## 3 Numerical simulation on short-term loading

### 3.1 Introduction

A parametric study on the load transfer between components in masonry using a continuum model was carried out. The presented simulation is part of a broader study with the aim of validating numerical models for the simulation of composite masonry under compression, in which both continuum and discontinuum models will be considered.

A non-linear finite element simulation has been carried out using DIANA finite element code [5], considering a representative volume element of regular

masonry under short-term compression. This element has been modelled with symmetry conditions in the boundaries and in plane stress (PS), plain strain (PE) and "enhanced plain strain" (EPE). EPE consists on modelling a masonry layer with 3D elements, imposing equal displacements in each face of the layer. In this way, out-of-plane displacements are allowed (unlike plane strain) but with a compatibility condition (unlike plain stress where the elements can deform freely out-of-plane). Full 3D analyses are unwieldy and will not be considered here.

The simulations carried out were compared with available experimental results on monotonically compressed specimens described in the next section.

### 3.2 Experimental results from Binda et al. [6]

Testing aimed at the evaluation of the mechanical compressive properties (strength and, axial and lateral deformations) of brick masonry prisms built with three different types of mortar. The prisms dimensions were 500×250×600 $mm^3$ and the solid soft-mud bricks dimensions were 250×120×55 $mm^3$. Mechanical properties found for brick, mortars and prisms are given in Table 1. Prisms MU1, MU2 and MU3 were built with mortars M1, M2 and M3, respectively.

Table 1. Mechanical properties of the masonry components and prisms.

| Specimen type | Compressive strength ($N/mm^2$) | Flexural tensile strength ($N/mm^2$) | Elastic modulus ($N/mm^2$) | Poisson ratio (-) |
|---|---|---|---|---|
| Brick | 26.9 | 4.9 | 4865 | 0.094 |
| Mortar 1 | 3.2 | 0.9 | 1178 | 0.057 |
| Mortar 2 | 12.7 | 3.9 | 5648 | 0.086 |
| Mortar 3 | 95.0 | 15.7 | 17758 | 0.115 |
| Prism MU1 | 11.0 | - | 1651 | 0.065 |
| Prism MU2 | 14.5 | - | 3833 | 0.0115 |
| Prism MU3 | 17.8 | - | 4567 | 0.0145 |

### 3.3 Material models and parameters used in the simulation

For plane stress and plane strain, a composite plasticity model with a Drucker-Prager yield condition in compression and a Rankine yield condition in tension was used. The value adopted for the friction angle $\phi$ was 10° (a larger value in plain stress would implicate an overestimation of the biaxial strength) and, for the dilatancy angle $\psi$, a value of 5° was adopted. The adopted inelastic behaviour is illustrated in Figure 4, exhibiting a parabolic hardening/softening diagram in compression and an exponential-like softening diagram in tension [5]. The material behaviour is elastic up to one-third of the compressive strength and up to the tensile strength.

The model described is not available for 3D models and, for "enhanced plane strain", a combined model with cracking in tension and plasticity (Drucker-Prager) in compression had to be used [5]. The models in tension are equivalent [7], but the plasticity-based model is numerically more robust.

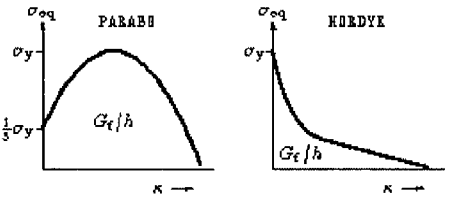


Figure 4: Adopted inelastic behaviour.

Table 2 presents all elastic and non-linear parameters adopted for the simulation. The values assumed for the fracture energy have been based in the experience of the authors.

Table 2. Material parameters.

| | Brick | Mortar 1 | Mortar 2 | Mortar 3 |
|---|---|---|---|---|
| Elastic modulus (N/mm$^2$) | 4865 | 1178 | 5648 | 17758 |
| Poisson ratio (-) | 0.094 | 0.057 | 0.086 | 0.115 |
| Tensile strength (N/mm$^2$) | 3.7 | 0.7 | 3.0 | 12.0 |
| Cohesion (N/mm$^2$) | 11.286 | 1.343 | 5.328 | 39.857 |
| $\phi$ (degrees) | 10 | | | |
| $\psi$ (degrees) | 5 | | | |
| Fracture energy (N/mm) * | 0.19 | 0.04 | 0.15 | 0.60 |
| Compressive fracture energy (N/mm) | 12.5 | 2.7 | 10 | 23 |

* To follow the complete stress-strain curve for Mortar 1, higher values of the fracture energy have been assumed for mortar and brick, respectively, 0.35 N/mm and 1.9 N/mm.

## 3.4 Numerically obtained results

### 3.4.1 Stress-strain curves

The stress-strain curves obtained in the numerical analysis are illustrated in Figure 5. The following observations can be made:

- The stiffness measured experimentally is approximately the half of the stiffness obtained in the numerical analysis. This is due to the mortar laying and curing. The fact that mortar inside the composite is different from mortar specimens cast separately represents a severe drawback of detailed micro-models. New analyses are necessary, adjusting the elastic stiffness of mortar by inverse fitting, so that the numerical stiffness is similar to the experimental stiffness.
- Experimental and numerical ultimate strains are rather similar.
- The diagrams corresponding to EPE are between the extreme conditions of PS and PE. The difference between the ultimate strength calculated in PS and PE, increases with the difference between the strength of the masonry components. Without any confining effect in the out-of-plane direction, the weaker material fails at an early stage, leading to masonry failure. In the rest of this paper, EPE is accepted as the reference solution.
- Numerical strength largely overestimates the experimental values obtained in all three prisms.

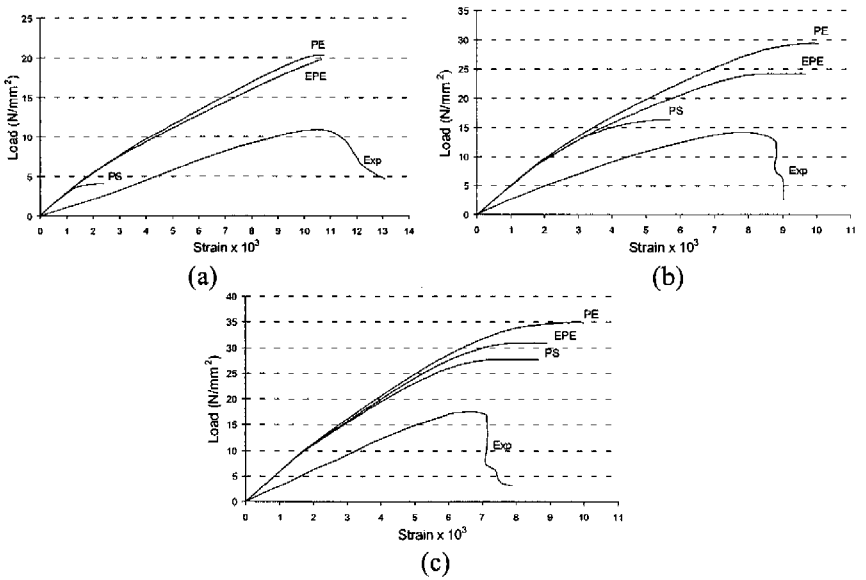


Figure 5: Experimental and numerical stress-strain curves in PS, PE and EPE conditions: (a) Prism MU1, (b) Prism MU2 and (c) Prism MU3.

### 3.4.2 Failure mechanisms

The obtained failure mechanisms depend on the model adopted. This is, of course, physically non-realistic but it is a key issue often disregarded.

In PS, prisms MU1 and MU2 fail due to crushing of the bed joints. In MU3 failure occurs due to the development of vertical cracks in the bed joints, together with diagonal cracks that cross the units and connect the non-aligned vertical cracks, see Figure 6.

In PE, prisms MU1 and MU2 fail due to vertical cracks that develop close to the middle of the bricks and in the head joints, with very limited diagonal cracks. For MU3, failure occurs with several vertical and diagonal cracks, that cross the joints and the units, see Figure 7.

In EPE, MU1 fails due to the development of vertical cracks in the bricks and in the head joints while MU2 fails due to crushing of mortar and bricks. MU3 fails due to the development of several vertical cracks that propagate from joints to the units, together with diagonal cracks that cross the bricks, see Figure 8.

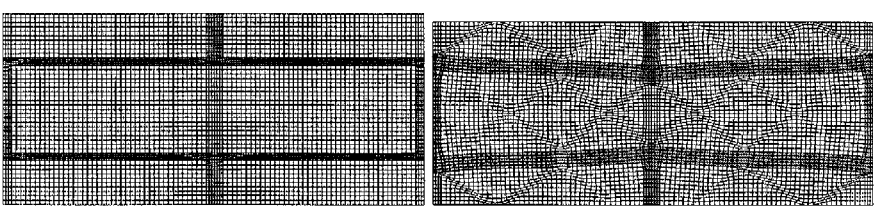


Figure 6: Deformed meshes at failure for PS, using incremental displacements, for (a) MU1 and (b) MU3.

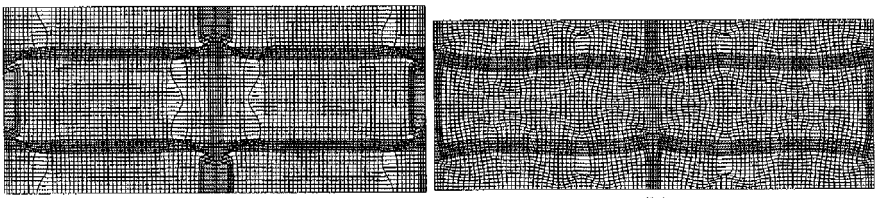

(a) (b)

Figure 7: Deformed meshes at failure for PE, using incremental displacements, for (a) MU1 and (b) MU3.

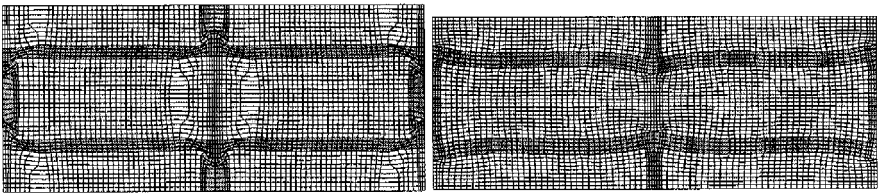

(a) (b)

Figure 8: Deformed meshes at failure for EPE, using incremental displacements, for (a) MU1 and (b) MU3.

### 3.4.3 Damage analysis

The damage in the prisms at failure has been analysed resorting to contour plots of the maximum plastic principal strains obtained in EPE, see a typical example in Figure 9. This gives also a good idea of the localization of cracks in the prisms.

The following observations can be made from the analyses:

- In prism MU1, damage is concentrated in the mortar joints rather than in bricks. The zones around brick corners are the most severely damaged.
- In prism MU2, the most damaged zones are located in the head joints and in the brick neighbouring faces as well around the brick corners.
- In prism MU3, which has a stronger mortar than brick, the units are more damaged and the zones more severely affected are the ones above the vertical mortar joint.

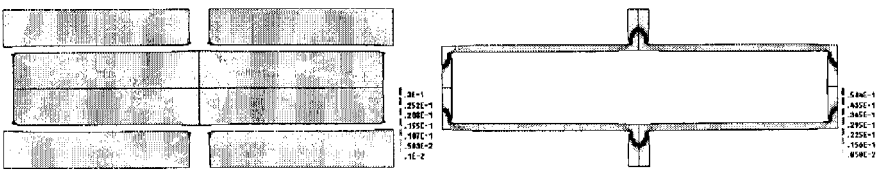

Figure 9: Maximum principal plastic strains in units and mortar joints for MU1 in EPE. The deformed shape corresponds to total displacements at failure. Higher damage corresponds to the darker colour.

### 3.4.4 Stress distribution analysis

The evolution of stress distribution in EPE along the material directions has been analysed considering three section lines that cross the structure, see Figure 10a.

Prism MU1 has been chosen as an example because it has a relatively strong unit and a rather weak mortar, as often occurs in ancient masonry. Three normal stress levels $\sigma$ were considered ($\sigma$ = 4.1, $\sigma$ = 14.0 and $\sigma$ = 19.8 N/mm$^2$), each one corresponding to different branches of the stress-strain curve.

The following observations can be made:

- Severe non-linear behaviour and stress redistributions occur. Failure does not coincide with attaining the maximum stress at a given point of the discretization.
- As expected, Figure 10b indicates that mortar is heavily triaxially compressed and brick is under combined compression – biaxial tension.
- A decrease of vertical compressive stresses in the bed joints is observed near the head joints due to the low mortar stiffness, see Figure 10c.
- A vertical stress concentration that rises with the load level develops in the brick edges, as the neighbouring head joint fails. Also due to this failure, the centre zone of the bricks exhibits a decrease of vertical stress, see Figure 10d.

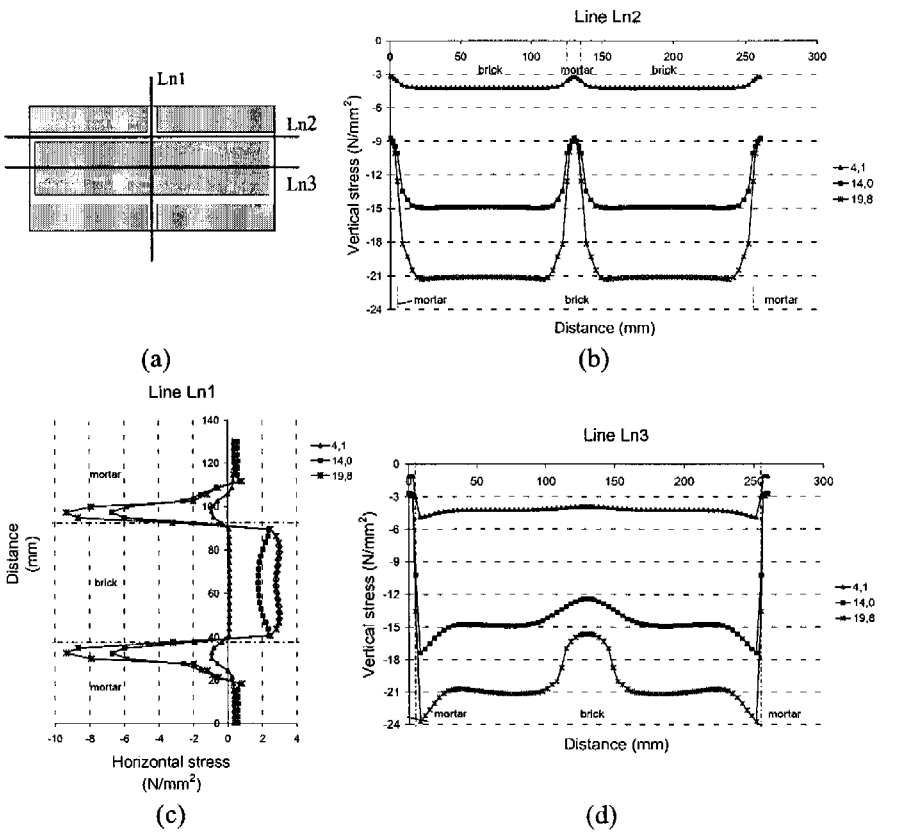


Figure 10: Stress distribution in the material directions along lines crossing the structure (EPE). Load level values are in N/mm$^2$.

### 3.5 Prism strength estimation using simplified numerical models

The strength of the prisms was estimated using two simplified models and also using the formula of EC6 [8]. The first method, developed by Lenczner [9] and Francis et al. [10], is based on the elastic analysis of a prism subjected to uniaxial compression, in which the unit is in compression – biaxial tension and the mortar is in triaxial compression. The second method was developed by Ohler [11] and also considers the elements in the referred states of stress. For this reason these two theories are only applicable in cases where the strength of brick exceeds the one of mortar, that is the case of MU1 and MU2. Both methods are described in Hendry [12]. For the application of EC6 to MU3, the mortar strength was assumed equal to 20 N/mm$^2$ (maximum value permitted by the code).

All results obtained are presented in Table 3. As it can be observed, all methods, excluding the empirical formula from EC6, overestimate the experimental strength values. Ohler method and EC6 yield the best strength approximations.

Table 3. Experimental and predicted strength values of prisms (N/mm$^2$).

| Prism | Tests | Lenczner [9] | Ohler [11] | EC6* [8] | Numerical simulation (EPE) |
|---|---|---|---|---|---|
| MU1 | 11.0 | 25.8 | 15.2 | 6.8 | 19.8 |
| MU2 | 14.5 | 27.3 | 19.4 | 9.6 | 24.2 |
| MU3 | 17.8 | - | - | 10.8 | 31.0 |

* The EC6 values were obtained considering a coefficient of variation of 10%.

## 4 Conclusions

The paper illustrates an integrated experimental – numerical approach aimed at the development of adequate design rules for the safety assessment and strengthening of historical masonry walls subjected to high compressive stresses.

The results obtained with a preliminary short term loading simulation of masonry prisms allow to conclude that: (a) continuum finite element modelling largely overestimates the experimental stiffness and strength of the prisms; (b) plane stress, plane strain and "enhanced plane strain" lead to different strengths and different failure mechanisms; (c) simplified methods to predict the strength based on elastic considerations provide different results from advanced numerical analyses and must be used with great care.

Tentative suggestions for further work are: (a) adopt "enhanced plane strain" or plain strain (up to 20% error) as modelling strategies, given the fact that parametric analysis are hardly possible with full 3D finite element models; (b) seek alternative models to represent the micro-structure of masonry components, so that reliable estimation of the masonry strength can be made; (c) develop an advanced experimental programme to characterize the mechanical behaviour of mortars inside a masonry composite.

# References

[1] van Zijl, G. Computational modelling of masonry creep and shrinkage. PhD thesis, Delft Univ. of Techn., 2000.
[2] Binda, L., Anzani, A., Mirabella Roberti, G. Long term behaviour of ancient masonries. *Construction materials – Theory and application*, pp. 253-262, 1999.
[3] Anzani, A., Binda, L., Melchiorri, G. Time dependent damage of rubble masonry walls. *Proc.4th Int. Masonry Conf.*, Vol. 2, No. 7, pp. 341-351, 1995.
[4] Binda, L., Anzani, A. The safety of ancient masonry towers: a survey on the effects of heavy dead loads. *Proc. Int. Conf. on Studies in Ancient Structures*, pp. 207-216, 1997.
[5] DIANA finite element code, Version 8.1, TNO Building and Construction research, The Netherlands, 2003.
[6] Binda, L., Fontana, A., Frigerio, G. Mechanical behaviour of brick masonries derived from unit and mortar characteristics. *Proc. 8th IBMaC*, Vol. 1, pp. 205-216, 1988.
[7] Lourenço, P.B., Rots, J.G., Feenstra, P.H., A tensile "Rankine" type orthotropic model for masonry. Proc. 3rd STRUMAS, p. 167-176. 1995.
[8] Eurocode 6, Design of Masonry Structures, Part 1-1, 1996.
[9] Lenczner, D. *Elements of load bearing brickwork*, ed. Pergamon: Oxford, 1972.
[10] Francis, A., Horman, C., Jerrems, L. The effect of joint thickness and other factors on the compressive strength of brickwork. *Proc. 2nd Int. Brick Masonry Conf.*, pp. 31-37, 1971.
[11] Ohler, A. Zur berechnung der druckfestigeit von mauerwerk unter berucksichtigung der mehrachsigen spannungszustande in stein und mortel. *Bautechnik*, Vol. 5, 1986.
[12] Hendry, A. Compression failure theories (Chapter 3). *Structural masonry*, ed. McMillan: UK, pp. 52-66, 1990.